Available online at www.sciencedirect.com
ScienceDirect
Trans. Nonferrous Met. Soc. China 32(2022) 1559−1574
Transactions of Nonferrous Metals Society of China
www.tnmsc.cn

Preparation of high-mechanical-property medium-entropy CrCoNi alloy by asymmetric cryorolling

Yu-ze WU[1,2,3], Zhao-yang ZHANG[1,2,3], Juan LIU[1,2,3], Charlie KONG[4], Yu WANG[4], Puneet TANDON[5], Alexander PESIN[6], Hai-liang YU[1,2,3]

1. State Key Laboratory of High Performance Complex Manufacturing, Central South University, Changsha 410083, China;
2. College of Mechanical and Electrical Engineering, Central South University, Changsha 410083, China;
3. Light Alloys Research Institute, Central South University, Changsha 410083, China;
4. Mark Wainwright Analytical Centre, University of New South Wales, Sydney, NSW 2052, Australia;
5. PDPM Indian Institute of Information Technology, Design and Manufacturing, Jabalpur 482005, India;
6. Laboratory of Mechanics of Gradient Nanomaterials, Nosov Magnitogorsk State Technical University, Magnitogorsk 455000, Russia

Received 12 April 2021; accepted 16 December 2021

Abstract: In order to obtain good strength−plasticity synergy for a medium entropy alloy (MEA) CrCoNi, cold rolling, asymmetric rolling, cryorolling and asymmetric-cryorolling with subsequent annealing at different temperatures were conducted. The results showed that the asymmetric-cryorolled alloy achieved a high strength of over 1.6 GPa. After annealing at 1073 K, it retained a high strength of ~1 GPa while the elongation reached nearly 60%. After annealing, the heterogeneous characteristics were formed in asymmetric-cryorolled samples, which were found to be more distinct than those of the samples subjected to asymmetric rolling. This resulted in the generation of high strength and ductility.
Key words: medium entropy alloy; heterogeneous structure; annealing; mechanical properties; asymmetric cryorolling

1 Introduction

Medium/high entropy alloys (MEAs/HEAs) are characterized by excellent mechanical properties, which have attracted immense attention from scientists and engineers [1]. Recently, WU et al [2] reported that the strength and ductility of equi-atomic MEA CrCoNi are higher than those of the HEA CoCrFeMnNi. The alloys have good combinations of strength and ductility in the temperature range from 77 to 673 K. Besides, the strengths of these MEAs increased as the temperature decreased [3]. LAPLANCHE et al [4] reported that nano-twinning in MEA CrCoNi occurred in larger strain ranges than in the five-element HEA CoCrFeMnNi, which improves the strength and ductility. GLUDOVATZ et al [5] achieved a balance between ultra-high strength and ductility in MEA CrCoNi, which has a tensile strength close to 1 GPa and a uniform elongation of 70%.

The thermomechanical processing (TMP) routes involve plastic processing and subsequent annealing [6] which significantly influence the mechanical properties of the material [7]. SUNKARI et al [8] reported that cryorolled HEA contains a larger density of potential heterogeneous nucleation sites than cold-rolled HEA. Cryorolled HEA had a heterogeneous structure composed of

Corresponding author: Hai-liang YU, Tel/Fax: +86-731-88879351, E-mail: yuhailiang1980@tom.com, yuhailiang@csu.edu.cn
DOI: 10.1016/S1003-6326(22)65893-X

residual deformation regions and recrystallization regions, which helped to increase the strength−plasticity synergy. REDDY et al [9] utilized a combined method involving cryorolling and warm- • rolling to prepare an HEA with structure−composition dual heterogeneous microstructure. And this HEA exhibited a combination of excellent strength and ductility. PATEL et al [10] studied the effect of different cryorolling routes on the structure, texture, and hardness of the eutectic HEA $AlCoCrFeNi_{2.1}$. The deformed structure appeared as a reserved lamellar structure area inherited from the cast structure of the eutectic HEA, and the rolled material exhibited an obvious heterogeneous structure. The results revealed that the TMP behavior exerts a significant impact on the performance of the HEAs [11]. Therefore, it is important to find a better TMP route to further improve the performance of the equi-atomic MEA CrCoNi, and other MEAs/HEAs with similar structures.

Cryorolling and asymmetric rolling are severe plastic deformation (SPD) technologies. Compared to other SPD technologies such as high-pressure torsion, cryorolling and asymmetric rolling can be used to process products with larger scales. The cryorolling [12,13] can effectively suppress the dynamic recovery of materials and improve the accumulation efficiency of dislocations. Conversely, high-density dislocations can also help generate a large number of nucleation sites during annealing. This results in the generation of finer grains [14,15] and increases the yield strength to the critical resolved shear stress of twinning. This significantly improves the strength of the material and can enhance the ductility of numerous metal-based materials [16,17]. WON et al [18] performed multi-pass caliber cryorolling on HEA CoCrFeMnNi and obtained ultra-fine grain (UFG) structures. BHATTACHARJEE et al [19] utilized the difference of stress partitioning in the constituent phases of cryorolled HEA to affect the stored energy and the driving force of the recrystallization process. The process resulted in the generation of a heterogenous microstructure in the eutectic HEA $AlCoCrFeNi_{2.1}$, leading to the simultaneous increase in the strength and ductility of the alloy. Asymmetric rolling is widely used to study the performance improvements of Ti, Al, and Cu sheets [20] and can also be used to fabricate HEA materials. HAN et al [21] conducted the asymmetric rolling and subsequent annealing process to prepare HEA CoCrFeNiMn with gradient structure and fine grains, which brought high back stress and work hardening, leading to high strength and ductility. JEONG and KIM [22] reported that incomplete recrystallization resulted in the bimodal heterostructure in the non-equi-atomic HEA produced by asymmetric rolling and annealing. The material exhibited a higher yield strength and better uniform elongation. However, the influence of asymmetric cryorolling on the properties of MEAs/HEAs is rarely studied.

In the previous studies on the equi-atomic MEA CoCrNi, some research believed solid solution strengthening [23] and the compositional dependence of the yield strength [24] could explain its superior performance. Apart from this, most of the studies indicated nano-twinning could be the main reason [4,25,26]. However, the critical stress of twinning at room temperature is quite high. Thus, it is difficult for the actual resolved shear stress to achieve. Based on the discussion above, the processes of cold rolling, asymmetric rolling, cryorolling, and asymmetric cryorolling were used to manufacture equi-atomic MEA CrCoNi in this study. And the rolled alloys were annealed at different temperatures.

2 Experimental

The experimental equi-atomic MEA CrCoNi ingots were vacuum arc-melted from the starting elements with purities higher than 99.9%, which were wire-cut to sheets with thickness of 1 mm. The distribution of Cr, Co, and Ni in the sample (Fig. 1) was characterized with a Bruker M4 Tornado X-ray fluorescence (XRF) spectrometer equipped with an Rh anode. The experiments were conducted under vacuum conditions, operated at 20 kV and 400 mA.

The as-cast sheets were cold-rolled (298 K), asymmetric-rolled (298 K, rolling speed ratio: 1.4), cryorolled (77 K), and asymmetric-cryorolled (77 K, rolling speed ratio: 1.4) to thickness of 0.2 mm. The sheets were rolled nine passes, and the total rolling deformation reached 80%. Table 1 presents the rolling process parameters. To ensure that cryogenic temperatures were maintained during the process of cryorolling, the samples were immersed in liquid nitrogen for more than 10 min before every rolling

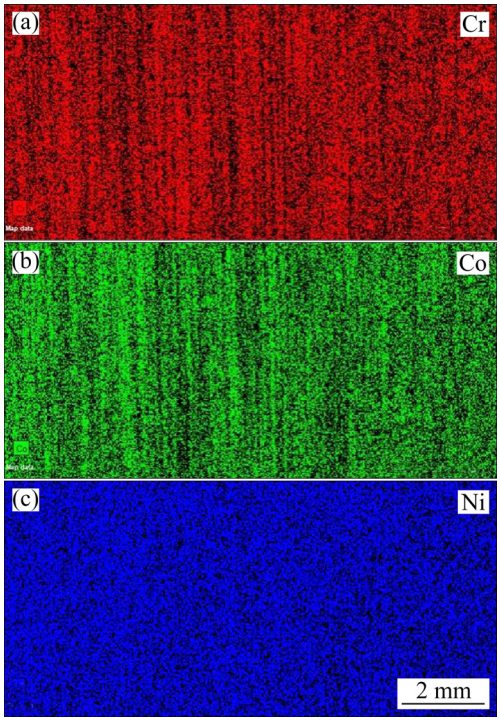

Fig. 1 XRF images of medium-entropy CrCoNi alloy: (a) Cr; (b) Co; (c) Ni

Table 1 Rolling process parameters

Rolling pass	Thickness/mm
1	1.00±0.01
2	0.92±0.02
3	0.83±0.03
4	0.75±0.04
5	0.63±0.04
6	0.52±0.02
7	0.43±0.04
8	0.29±0.04
9	0.20±0.01

pass. Then the specimens were annealed at 873, 973, and 1073 K for 30 min, followed by air cooling.

The mechanical properties of the samples were measured using an AGS-X 10 kN tensile tester (Shimadzu, Nakagyo-ku, Kyoto, Japan) at room temperature with a tensile rate of 1×10^{-3} s^{-1}. Three samples from each group were selected and stretched under the same experimental conditions. The tensile specimens had the following dimensions: parallel length of 16 mm, width of 2.5 mm, and thickness of 0.2 mm.

A Philips CM200 field emission gun transmission electron microscope (FEG-TEM) operating at 200 kV was used to examine the microstructures of the specimens in the planes of the rolling and normal directions. A Thermo Fisher Helios G4 PFIB was used to prepare the TEM specimens from the rolled samples with an in-situ lift-out technique. The post-focused ion beam (FIB) specimen process was carried out using a Fischione 1040 Nanomill operating at 500 V and 180 μA at a tilt angle of ±10° after polishing each side for 2 min. The digital micrograph software was used to measure the randomly selected grain size. One hundred grains were used to generate the grain size distribution result. The microstructures of the annealed materials were characterized using an electron backscatter diffraction (EBSD) system (Oxford Instruments, Nordlys, Abingdon, Oxfordshire, UK) in Institute of Metal Research, China. The step size for the EBSD measurements was 0.0754 μm. The material was first polished mechanically. Then, it was ion-etched using a Leica RES101 ion-etcher (Leica Microsystems, Ernst-Leitz-Strasse, Wetzlar, Germany). Subsequently, it was analyzed using an OXFORD Nordlys Nano EBSD camera and Channnel5 processing software to obtain the EBSD results. The fracture surfaces of the tensile test specimens were analyzed using a TESCAN MIRA3 scanning electron microscope (SEM). A PANalytical Powder diffractometer, Empyrean II system with Co as the anode, operating at 45 kV and 40 mA, was used to analyze the phase structures of the materials.

3 Results

3.1 Phase identification and phase stability

The as-cast MEA CrCoNi exhibited a single FCC structure and a stable phase structure even in the temperature range of 1200−1500 K. The average valence electron concentration (VEC) is a reliable descriptor for the prediction of the crystal structure, and it is given as follows [27]:

$$\mathrm{VEC}=\sum_{i=1}^{n}c_i(\mathrm{VEC})_i \tag{1}$$

where $(\mathrm{VEC})_i$ is the VEC of the ith element, and c_i is the concentration of the element. The VECs of Co, Cr, and Ni were 9, 6, and 10, respectively [27]. The VEC of the equi-atomic MEA CrCoNi was calculated as 8.33, similar to that of HEA

CoCrFeMnNi [28]. According to ZADDACH et al [29], the FCC phase is more stable when the VEC is greater than 8. This indicates that the stability of the FCC phase of the MEA CrCoNi is slightly better than the stability of HEA CoCrFeMnNi.

Figure 2 shows the XRD diagrams of the rolled MEA CrCoNi. The lines in Figs. 2(a−d) represent the full widths at half maximum (FWHM) for samples subjected to the process of cold rolling, asymmetric rolling, cryorolling, and asymmetric cryorolling, respectively. These samples exhibited single FCC solid-solution structures, indicating that asymmetric rolling and cryorolling did not change the phase compositions of the alloys. It was observed that after the process of annealing, the composition of the recrystallized phase did not change.

Figure 3 shows the phase maps of the alloy, which reveals that the primary phase was FCC. The presence of a small amount of the BCC phase was also observed in EBSD diagram but not in XRD

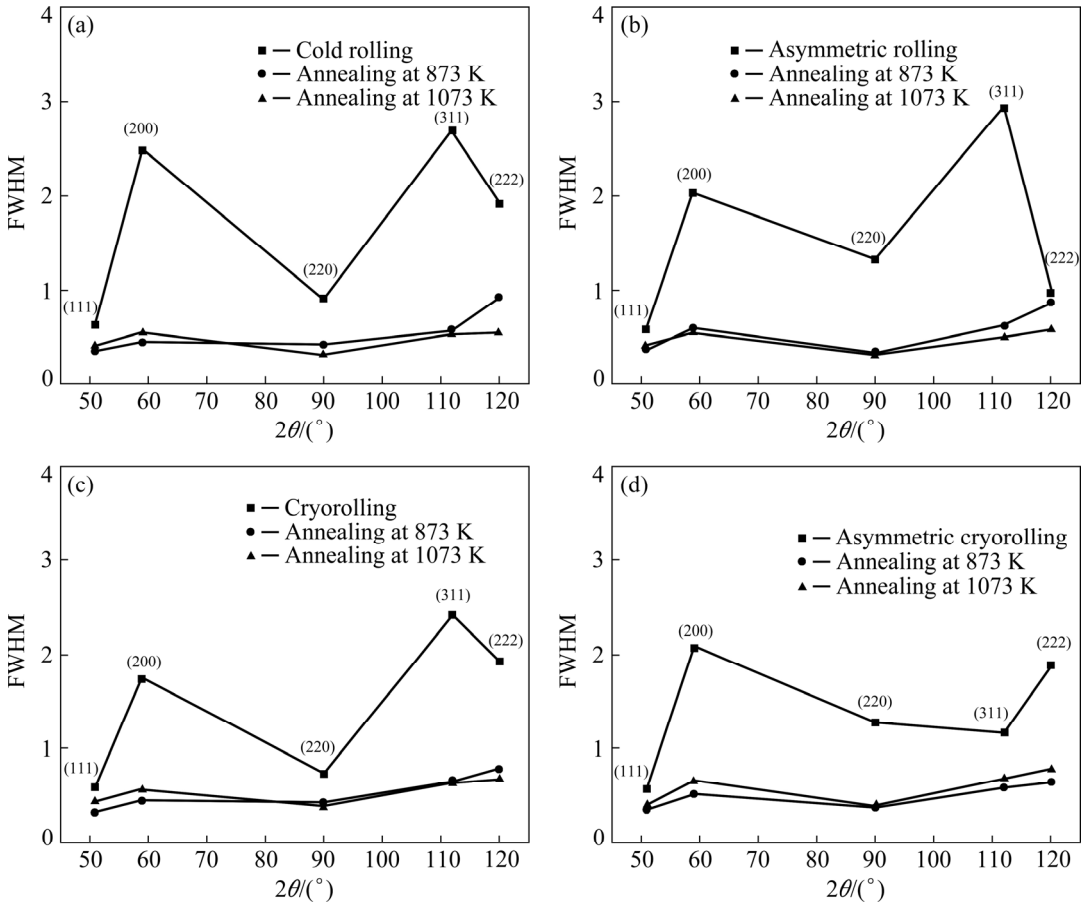

Fig. 2 XRD peak FWHM measurements of MEA CrCoNi subjected to different processes: (a) Cold-rolling; (b) Asymmetric rolling; (c) Cryorolling; (d) Asymmetric cryorolling

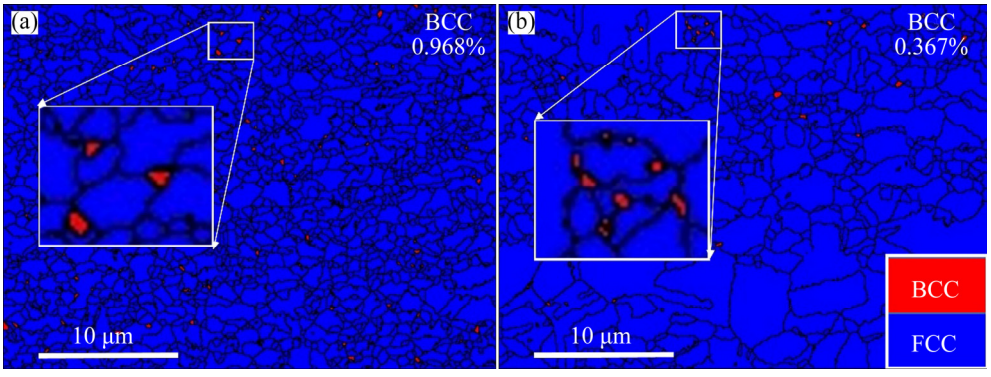

Fig. 3 Phase maps of CrCoNi via asymmetric cryorolling followed by annealing at 873 K (a) and 1073 K (b)

patterns. When the annealing temperature was 873 K, the material contained 0.968% BCC phase, and when the annealing temperature was increased to 1073 K, the proportion of the BCC phase decreased to 0.367%. MORAVCIK et al [30] also observed the existence of BCC phase at the grain boundary of the equi-atomic MEA CrCoNi. LIANG et al [31] also detected BCC phases with a volume fraction of ~6% in a precipitation-hardened high entropy alloy with ultra-high strength, and the BCC phases were Cr-rich lamellar phases. They calculated the forecast value of the BCC contribution to the strength, which was similar to the actual value obtained from experiment. WANI et al [32] reported that the microstructure of the cold-rolled and annealed eutectic HEA $AlCoCrFeNi_{2.1}$ was coarser than that of the as-cast alloy. However, the former was stronger than the latter. This could be partially attributed to the increase in the BCC phase content. SHI et al [33] constructed a two-stage heterogeneous eutectic HEA consisting of micron-grade alternate FCC/B2 lamellae. It was also observed that the micron-grade FCC lamellae consisted of submicron-grade FCC/BCC grains. These results illustrated that the BCC phase not only exerted a strengthening effect but also hindered the deformation of heterogeneous structure. This also contributed to the back-stress-strengthening effect. In addition, Fig. 3 reveals that BCC phase mainly appeared at the triple junction, grain boundaries, and the annealed twin boundary, which is similar to the past reports [34]. Larger and higher proportion of the BCC phase particles were also observed at the triple junction compared to the grain boundary. However, the BCC phase particles were rarely observed at the twin boundary. The contents of the BCC phase followed the trend: triple junctions < grain boundaries < non-coherent twin boundaries < stack faults < coherent twin boundaries < dislocations [35]. The positions and size of the BCC phase were analyzed to better understand the formation mechanism of the second phase. However, compared to the entire FCC matrix, the proportion of the BCC phase was very small. Therefore, the second phase enhancement effect is neglected in the subsequent analysis of the deformation-strengthening mechanism.

3.2 Microstructure produced following rolling and annealing processes

Figures 4(a, b, d, e) show the TEM images of MEA CrCoNi subjected to cold rolling, asymmetric

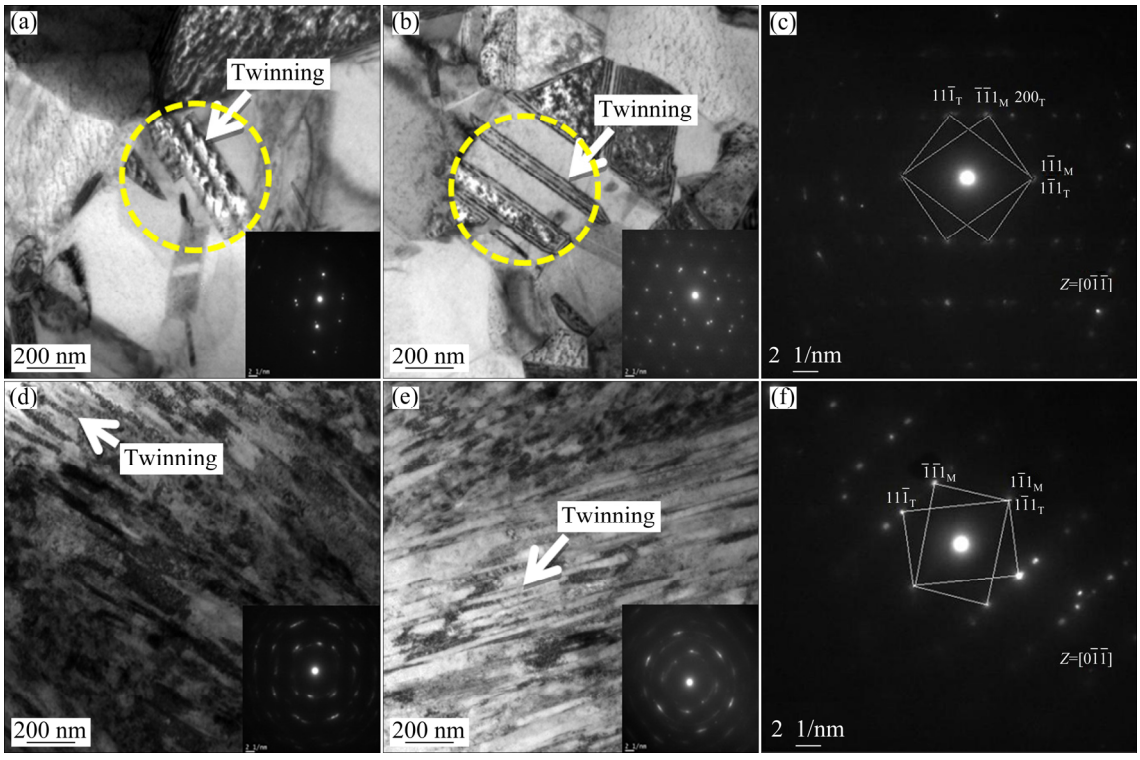

Fig. 4 TEM images of MEA CrCoNi: (a) After cold rolling; (b) After asymmetric rolling; (c) Cold-rolled CrCoNi twinning diffraction spot; (d) After cryorolling; (e) After asymmetric cryorolling; (f) Asymmetric-rolled CrCoNi twinning diffraction spot

rolling, cryorolling, and asymmetric cryorolling processes, respectively. The all show the effect exerted by severe cold plastic deformation on the alloy (a large number of tangled dislocation cells with small regions and high density were evident). The grains observed in the TEM image of the asymmetric-rolled alloy were smaller than the grains in symmetric-rolled alloys. The dislocation cells produced by cryorolling were denser than those formed in cold rolling, and the degree of grain size reduction was also more significant. This indicated that cryorolling introduced greater deformation intensity, resulting in significant grain refinement. The extent of grain refinement achieved was greater in this case than the extent of grain refinement achieved with asymmetric rolling. Selected area diffraction (SAD) patterns of each region are shown at the lower right corner of each figure. The SAD pattern of the alloys produced by cold rolling and asymmetric rolling indicated that the rolled alloy exhibited a simple FCC structure. These results were consistent with the results presented in Fig. 2. The SAD pattern of cryorolled and asymmetric cryorolled alloys changed from a typical single crystal diffraction pattern to circular nanocrystal diffraction patterns composed of diffraction spots. This indicated that the structure was polycrystalline with various crystal orientations. This further confirmed the significantly finer grains observed in TEM image. The SAD patterns of the asymmetric-rolled samples tended to form a complete polycrystalline diffraction ring, indicating that the internal stress was higher in the material and the difference in the neighboring grain orientation was also larger.

Figure 5 shows the EBSD images of the rolled MEA CrCoNi samples after annealing at 873 K and 1073 K. The coordinates presented at the upper right corner of Fig. 5 indicated that the EBSD shooting position was the transverse direction (TD) plane formed by the normal direction (ND) and rolling direction (RD).

The small grain size produced after annealing could be attributed to the influence of the lattice distortion and sluggish diffusion on the recrystallization rate. The lattice distortion effect reduced the driving force for the nucleation and growth of new grains. The sluggish diffusion effect suppressed the grain boundary mobility, synergistically reducing the recrystallization rate and inhibiting the growth of the recrystallized grains. The significantly low stacking fault energy (SFE) of the MEA CrCoNi resulted in a greater extent of twinning in the material, and the severely fractured microstructure provided more potential nucleation sites for recrystallization [32]. As the annealing temperature increased, the externally applied thermal energy gradually offset the abovementioned effect which suppressed grain growth. The growth of grains was evident in the samples annealed at 1073 K. The color distribution observed in the 873 K-annealed alloys was rather messy, showing no evident trend toward the formation of a certain crystal plane. As the annealing temperature increased, the orientation of a large number of grains changed toward the same plane orientation, indicating that the annealing temperature affected the orientation distribution of the recrystallized grains. Furthermore, the proportion and sizes of the recrystallized grains increased simultaneously. In addition, distinct annealing twinning was evident in the coarse recrystallized grains.

3.3 Mechanical properties after rolling and annealing

Figure 6 shows the tensile strength and fracture elongation of the MEA CrCoNi subjected to four kinds of rolling processes and subsequent annealing. Excellent mechanical properties were observed in the asymmetric-cryorolled MEA CrCoNi samples. The strength was well above 1.6 GPa while a fracture elongation of 19% was maintained. In addition, the conventional change in the mechanical properties caused by recrystallization following heat treatment was observed in all four cases. As the annealing temperature was increased, the degree of recovery and recrystallization of the alloy increased, and the stress generated during rolling decreased. Furthermore, the density of the dislocations produced during the recrystallization process gradually decreased under these conditions. As the annealing temperature increased, the tensile strength decreased, and the fracture elongation increased, showing a stronger strain hardening ability. The ductility of the asymmetric-cryorolled alloy annealed at 873 K could be significantly improved, which was approximately double that of the unannealed alloy, while the strength still remained at a high value of 1153 MPa. When the

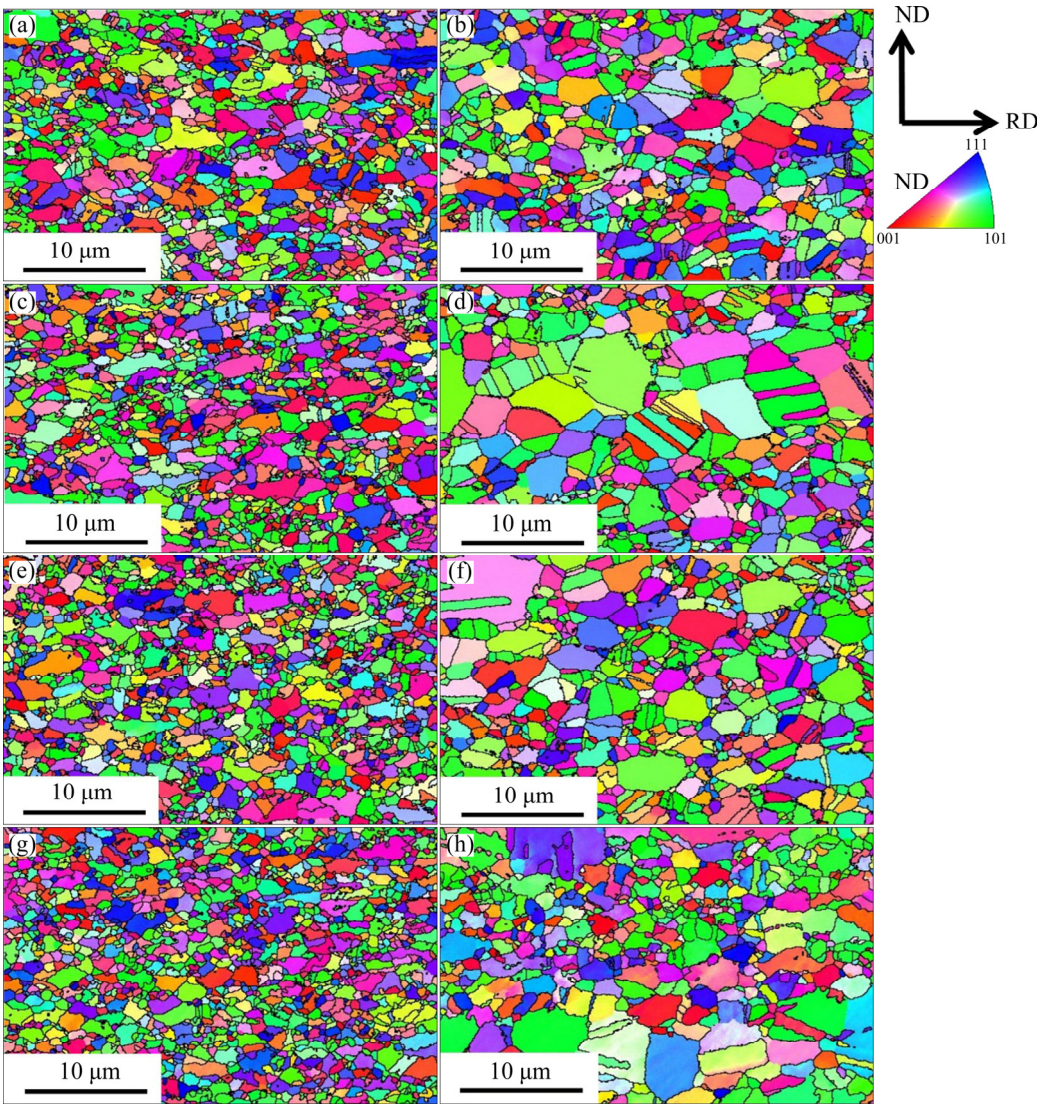

Fig. 5 EBSD orientation imaging maps of MEA CrCoNi sample subjected to different processes and annealed at 873 K (a, c, e, g) and 1073 K (b, d, f, h) for 0.5 h: (a, b) Cold rolling; (c, d) Asymmetric rolling; (e, f) Cryorolling; (g, h) Asymmetric cryorolling

annealing temperature reached 973 K, the fracture elongation increased significantly. At this time, the tensile strength of the alloy was 1047 MPa. The tensile strength of the sample annealed at 1073 K reached 966 MPa, while the fracture elongation exceeded 57%.

Figure 7 shows tensile fracture morphologies of the specimens. The fracture morphologies of the specimens all represented the characteristics of the typical dimple fracture. Thus, these fractures were basically plastic fractures. Although there were no significant differences in the dimensions, the dimple size distribution was more uniform on the asymmetric-rolled sample compared to the distribution observed in other samples. The dimple size was universally larger than that observed in the symmetric specimen. A deeper and denser dimple morphology can also be clearly seen, resulting in the better ability to absorb plastic deformation energy. The results reflect the tensile mechanical properties reported earlier (the fracture elongation of the asymmetric-rolled specimen was higher than that of the symmetric-rolled specimen). The cryogenic conditions helped produce significantly larger (the average size of the dimples of the asymmetric-cryorolled specimen was in the range of 3−11 μm, while that of the asymmetric-rolled specimen was in the range of 1−6 μm), deeper, and denser morphologies, which corresponded to better plastic toughness. It has already been concluded

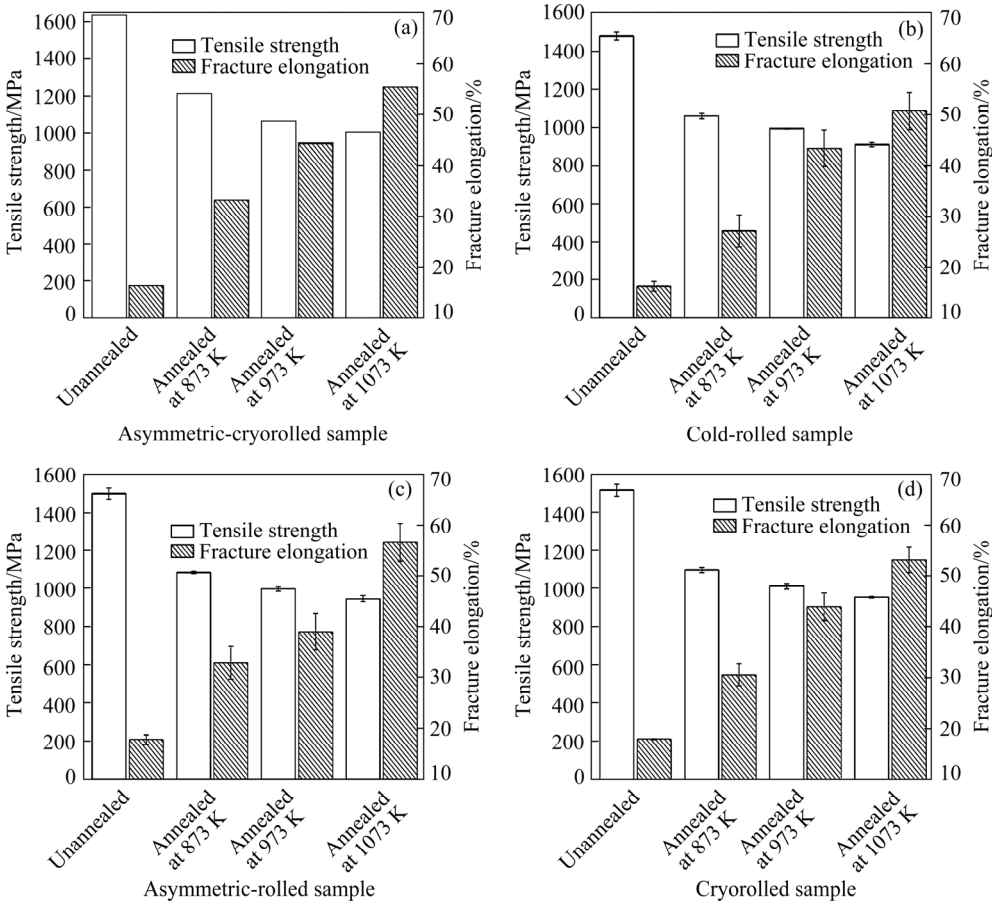

Fig. 6 Mechanical properties of alloys subjected to asymmetric cryorolling (a), cold rolling (b), asymmetric rolling (c), and cryorolling (d) after different annealing treatments

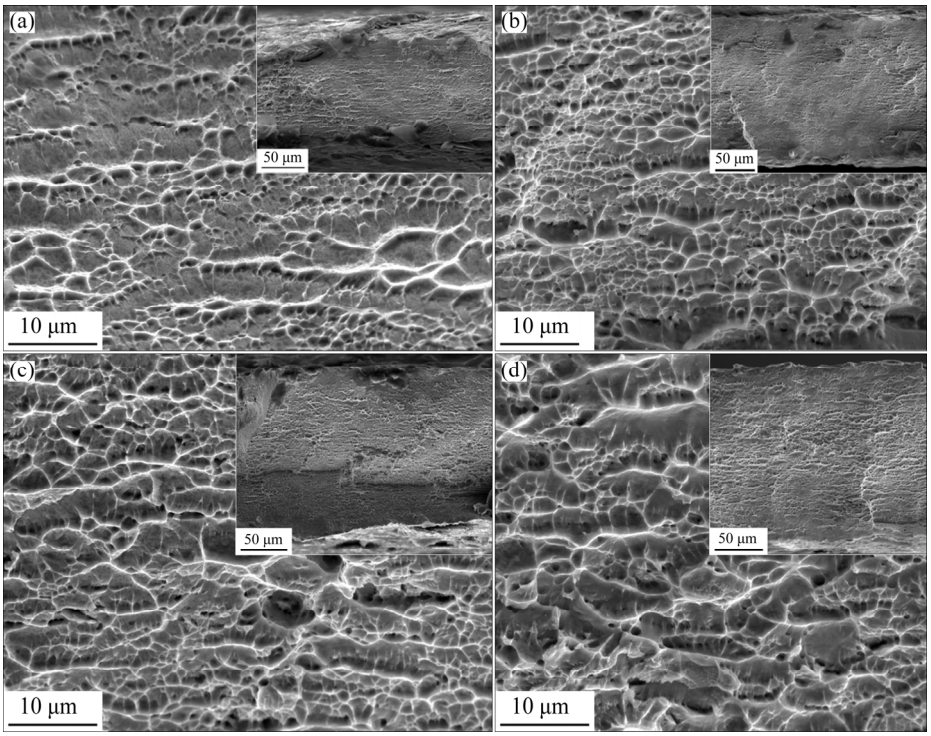

Fig. 7 SEM images of fracture morphologies of cold-rolled (a), asymmetric-rolled (b), cryorolled (c), and asymmetric-cryorolled (d) samples

that the dimple morphology was affected by the rolling-speed ratio earlier. The effect of the cryogenic treatment conditions on the depth and density of a dimple of the rolled part was larger than the effect generated by the rolling speed ratio. The microscopic morphology reveals that the strengthening effect of the cryogenic treatment process on the plastic toughness was larger than the effect generated by the rolling-speed ratio. Figure 8 shows the morphologies of the dimples annealed at 1073 K. As the annealing temperature increased, the dimples became deeper and denser. The results were consistent with the increase in ductility.

4 Discussion

4.1 Effect of rolling processes on hetero-structured microstructure

Figure 9 shows the grain size distribution in the alloys produced by cold rolling and asymmetric rolling. The average grain size of the cold-rolled material was 552 nm, and most of grains are in the size range of 600−699 nm. In contrast, the average grain size of the alloys via asymmetric rolling was 466 nm, and most of grain sizes were mainly in the range of 300−399 nm. This shows that the grain

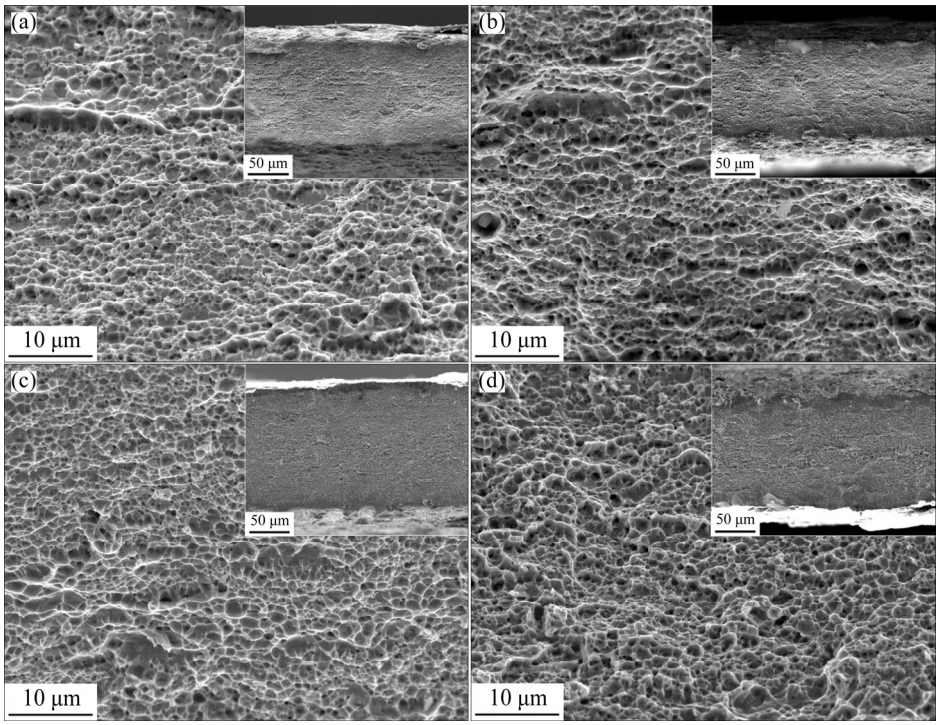

Fig. 8 SEM images of fracture morphologies of different samples annealed at 1073 K: (a) Cold-rolled; (b) Asymmetric-rolled; (c) Cryorolled; (d) Asymmetric-cryorolled

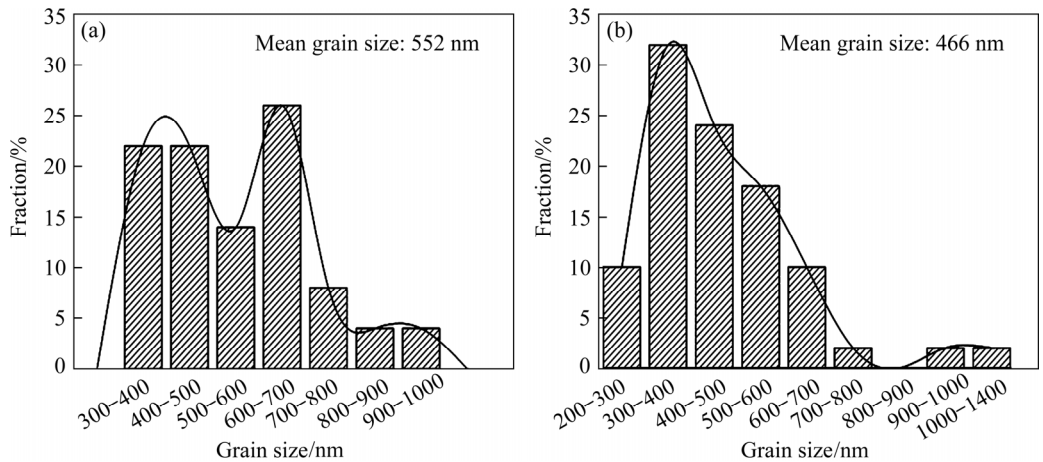

Fig. 9 Grain size distribution of cold-rolled (a) and asymmetric-rolled (b) MEA CrCoNi

size in asymmetric-rolled alloy was significantly smaller than that observed in the cold-rolled alloy. However, a lamellar structure with severe deformation was formed in the alloy by cryorolling. Therefore, the specific dimensions of the alloy grains are not discussed due to the small fine lamellar spacing and tangled dislocations. Based on the analysis of the grain spacing observed in the TEM image and the TEM ringed diffraction patterns mentioned earlier, it was believed that nanocrystals were obtained in this region by cryorolling. Moreover, the heterogeneous lamellar structure was observed in the alloy after asymmetric cryorolling. The lamellae in some regions had smaller spacings than others, and the soft lamellar structures were heterogeneously dispersed in the hard matrix, forming a heterogeneous lamellar structure. As reported by WU et al [36], the heterogeneous lamellar structure obtained with asymmetric rolling could be attributed to the variation in the slip systems and plastic strain in grains exhibiting different initial orientations. The TEM images shown in Fig. 4(e) also indicate that the dislocation density in the coarse lamellae was relatively low. This is consistent with the characteristics of the heterogeneous lamellar structure, which is responsible for the generation of a strain gradient between the soft and hard lamellae.

STEPANOV et al [37] studied the tensile properties of HEA CrMnFeCoNi at 298 and 77 K and found that the tensile strength of the alloy at the cryogenic temperature can be as high as 1500 MPa. The tensile strength recorded at 77 K was higher than the tensile strength of the alloy recorded at 298 K. The increase in the strength was influenced by the ratio of twinning and the higher strain range of twinning. The stacking-fault energy of the MEA CrCoNi was significantly low ((22±4) mJ/m^2) [4], which was 25% lower than the value of HEA CrMnFeCoNi [38]. This indicated that the MEA CrCoNi was likely to form the deformation twinning [25]. Correspondingly, twinning was evident in the TEM images of both the cold-rolled and asymmetric-rolled specimens. Figures 4(c, f) show the diffraction spots of the cold-rolled and asymmetric-rolled samples, respectively, confirming the presence of twinning. Twinning introduced twin boundaries. The generation of a large number of interfaces results in a decrease in the dislocation mean free path, which enhances the strength. The strengthening effect exerted by the twin boundary was similar to that exerted by the high-angle grain boundary. The increase in the yield strength attributed to the twin boundary can also be determined according to Hall–Petch equation as follows:

$$\sigma_y = \sigma_0 + k_{TB}\lambda^{-1/2} \quad (2)$$

where σ_y is the yield strength attributed to the twin boundary, σ_0 is lattice friction resistance, k_{TB} is a constant, and λ is the average twin thickness. Therefore, enhanced twinning in the specimen also results in increased alloy strength. A large number of dislocations pile up under these conditions. Storage dislocations can be generated in the twin interface induced by deformation, increasing the strength and ductility simultaneously [39]. However, according to previous research [40], a large number of sessile dislocations in the twinning can promote strain hardening, thereby delaying the onset of necking and improving the uniformity of elongation achieved before fracture. LIU et al [41] reported that the low stacking fault energy (SFE) of the MEA CrCoNi sample resulted in a decrease in the thickness of the deformation-twinning width and better mechanical performance. SATHIARAJ et al [42] studied MEA CrCoNi that was annealed at 973 and 1373 K following the process of cold rolling. A large number of annealing-twins were observed in all the samples, and the content of twins increased significantly at 1373 K. According to the Fullman and Fischer theory [43] of the formation of annealing-twinning, annealing twins are driven by the constant migration of the triple points. The content of annealing twinning increases as the recrystallized grain size increases. Studies on CrCoFeMnNi HEA by OTTO et al [44] also revealed that the content of twins was significantly influenced by the extent of the grain growth. BHATTACHARJEE et al [45] studied the evolution of the grain boundaries of pure nickel sintered at 1173, 1373 and 1573 K. They found that when the sintering temperature increased, the grain size increased, and the proportion of the Σ3 boundary also increased, indicating a growth in the content of annealing twins. WU et al [46] reported that the grain size reduction resulted in a decrease in the thickness of the twin and an increase in the twin spacing, which strongly inhibited the twin activities of the recrystallized alloys. The smaller the

thickness of twinning was, the smaller the slip dislocations that could pass through the nanoscale twin were. The effect of the strain hardening by twinning was weakened as the twin spacing increased. Thus, an increased extent of grain refinement hindered the promotion effect of twinning, resulting in a decrease in the hardening ability.

Twinning could not be observed clearly in the TEM images (Figs. 4(d, e)) for cryorolled samples. This could be attributed to the small grain size and high dislocation density. High-resolution TEM images were recorded to confirm twinning. Figures 10(a, b) and 10(c, d) correspond to samples by symmetric rolling and asymmetric rolling at cryogenic temperatures, respectively, which confirm the presence of high-density deformation twinning. The results agree well with the results reported by LAPLANCHE et al [4]. More deformation-induced twinning was found in the low-temperature deformation of the MEA CrCoNi and HEA CoCrFeMnNi FCC materials than in the corresponding room-temperature-deformed materials.

Theoretically, the recrystallization temperature decreases as the extent of plastic deformation of the alloy increases. And the recrystallized grain sizes decrease at the same time [47]. Correspondingly, as shown in Fig. 5, the grain size of the asymmetric-rolled and 973 K-annealed sample was smaller than the grain size of the cold-rolled and 973 K-annealed sample. The results indicated that the extent of deformation in asymmetric-rolled samples was larger than the extent of deformation observed in cold-rolled samples when the rolling reduction and number of rolling passes were the same. When the annealing temperature reached 1073 K, a more distinct heterostructure appeared in asymmetric-rolled specimen, in which lamellar structure consisting of coarse soft grains and lamellar

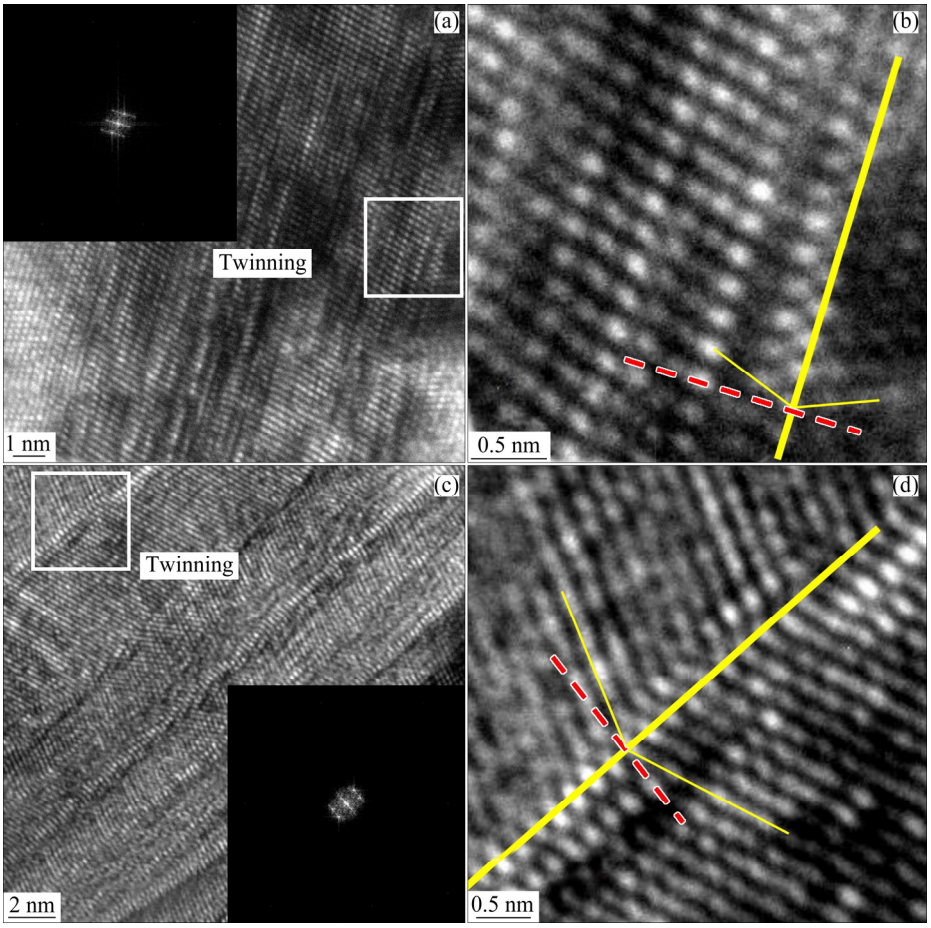

Fig. 10 HRTEM micrograph of deformed nanostructure of cryorolled MEA CrCoNi (a) with enlarged view showing deformation twinning (b), and HRTEM micrograph of deformed nanostructure of asymmetric-cryorolled MEA CrCoNi (c) with enlarged view showing deformation twinning (d) (The electron beam directions for both micrographs are close to ⟨110⟩)

structure consisting of fine grains superimposed on each other, forming a heterogeneous lamellar structure. The coarse lamellae were easier to deform plastically under conditions of plastic deformation (compared to the fine lamellae), while the fine lamellae remained elastic and acted as a constraint on the coarse layer. Due to the continuity of the strain among different regions, there were plastic strain gradient in the areas between two different lamellae, which needed to be adjusted by geometrically necessary dislocations (GNDs). The GNDs stacking at the interface generated a back stress which obstructed the dislocations from moving in grains, increasing the yield strength. The interaction between the large and small grains promoted the formation of multiaxial stress states, which stimulated the spatial nucleation of new GNDs, accelerating the activity of new slip systems and improving the ductility of the material [48].

Distinct grain refinement can be observed in the EBSD maps for the cryorolled and annealed specimen, with a significantly smaller grain size than the grain size of cold-rolled and annealed samples. This explains the relationship of the mechanical properties mentioned above. Unlike asymmetric-rolled material, the presence of heterogeneous lamellar structure was not observed in cryorolled materials, indicating that the generation of a heterostructure does not depend on the process of cryorolling. The coarse grains of the asymmetric-cryorolled alloy after annealing at 873 K formed a lamellar structure that was distributed in the fine lamellae. The proportion of fine grains was also larger, and the size was smaller than that of the former, which proved that the process of asymmetric cryorolling helped maximize the extent of plastic deformation of the alloy under the same rolling procedure (same rolling passes and rolling reduction). When the sample was annealed at 1073 K, the coarse lamellae in the heterostructure grew significantly at the high annealing temperature, but the alloy retained the distinct fine-grain lamellae under these conditions. The asymmetric-cryorolled alloy exhibited a two-stage structure that was more distinct than the structure in the asymmetric-rolled alloy after annealing at 1073 K. The load transfer and elastic−plastic transformation characteristics of the strain distribution among the grains of different sizes resulted in an increase in the rate of strain-hardening. As a result, a larger strain gradient appeared between the soft and hard domains. This resulted in the production of more numbers of GNDs that helped adjust the strain gradient. This also promoted back stress to further improve the material properties.

4.2 Influence of heterostructure microstructure on mechanical properties

In general, the work hardening of metal-based materials is primarily influenced by the dislocation density. According to the Taylor hardening relationship, the formula for calculating the flow stress and dislocation density [49] is as follows:

$$\sigma = CGb^2\sqrt{\rho} = CGb^2\sqrt{\rho_S + \rho_G} \tag{3}$$

where σ is the flow stress, C is a constant, G is the shear modulus, b is the magnitude of Burgers vector, and ρ is the dislocation density. ρ can be classified into statistically stored dislocations ρ_S and geometrically necessary dislocations ρ_G. ρ_S is related to the equivalent plastic strain arising from the mutual attraction of dislocations. ρ_G is related to the plastic strain gradient attributed to the unequal extent of deformation inside the material [50]. For traditional homogeneous materials, dislocations represent statistically stored dislocations. However, for heterogeneous materials, a significant influence of GNDs on back stress is observed which may even be much larger than the strengthening effect exerted by the equivalent plastic strain [36].

FU et al [51] prepared HEAs exhibiting the single-phase FCC structure with the processes of hot rolling, cold rolling, and annealing. The properties of the hot-rolled thick plates (coarse-grained (CG) materials) were compared with those of the annealed heterostructure materials. It was found that the plasticity of the heterostructure was similar to that of the CG material, while the yield strength of the former (350 MPa) was approximately double that of the latter (614 MPa). This revealed a high work-hardening ability. Furthermore, the breaking strength reached 1308 MPa. SHI et al [33] used a eutectic HEA $AlCoCrFeNi_{2.1}$ and designed a two-phase microstructure of ultrafine grains with the process of rolling and annealing. The process yielded a heterogeneous lamellar structure with a high interface density from the as-cast state. Two-phase strengthening inside the lamella was also observed. Under the effect of the two-stage strain partitioning

process, the yield strength of the alloy could reach 1.5 GPa, while the plasticity was still 16%, performing an improved strength and a well-balanced ductility. CHEN et al [52] produced a gradient hierarchical structure (GHS) by subjecting HEA $Al_{0.1}$CoCrGeNi to the cyclic dynamic torsion (CDT). Materials with coarse, intermediate, and fine-grained regions showed superpositions over individual regions. The mechanical properties obtained were better, and a synergistic enhancement was observed. The researchers attributed the heterogeneous structure to the back-stress strengthening effect. In addition, it was observed that GHS materials exhibited excellent twinning activities. SLONE et al [53] cold-rolled and annealed equi-atomic MEA CrCoNi, resulting in the production of a partially recrystallized heterogeneous microstructure, which significantly improved the yield strength and ductility of the alloy (1100 MPa and 23%). The strength and ductility of the material were compared with those of the equi-atomic MEA CrCoNi subjected to high-pressure torsion (HPT) and annealing by YOSHIDA et al [54]. It was found that the heterostructure alloy exhibited better uniform elongation properties than the homogeneous ultrafine-grained alloy while having a similar strength.

Among these four kinds of rolling processes, the tensile strength of the cold-rolled sample at room temperature could reach 1478 MPa, and that of asymmetric-rolled sample reached 1498 MPa, with an increase in ductility of more than 2%. The tensile strength of the cryorolled alloy could reach up to 1513 MPa, while the tensile strength of the alloy subjected to asymmetric cryorolling could further increase to 1612 MPa. A slight increase in the ductility was also observed in the latter. Both the strength and ductility of the alloy subjected to asymmetric rolling were superior to those of the symmetric-rolled alloys. The properties of the cryorolled alloys were better than those of the alloys subjected to room temperature rolling. XIA et al [55] reported that asymmetric rolling helped tilt the texture orientation toward the plane of the matrix. This promoted plastic deformation. MA et al [56] also reported that asymmetric rolling could refine the grains, improving the strength and ductility of the material. SARMA et al [57] concluded that the deformation of alloys with low stacking fault energy generally relies on twinning, while alloys characterized by high stacking fault energy tend to deform by slip dislocations. Most of the metals with stacking fault energies between high and low values deform by dislocation slip during the process of cold rolling. And twinning deformation occurs during the process of cryorolling, which allows cryorolling to enhance the strength and ductility of the alloy. The extent of increase is more than that achieved by the process of cold rolling. The results are consistent with the equations presented in the discussion above. YU et al [58] studied the Ti−6Al−4V alloy that was subjected to the processes of asymmetric cryorolling, asymmetric rolling, and cold rolling. They also reported that the alloys obtained via asymmetric cryorolling exhibit significantly better mechanical properties than the alloys subjected to asymmetric rolling and cold rolling. This can be attributed to the strong grain refinement effect, second phase size reduction, and higher dislocation density accumulation. Analyses of the grain size, SAD pattern, fracture morphology, and damage tolerance revealed that the high-ductility strengthening effect produced during cryorolling was larger than that produced during asymmetric rolling.

In addition, Fig. 6 reveals that the strength and fracture elongation increased in turn for cold-rolled, asymmetric-rolled, cryorolled, and asymmetric-cryorolled alloys after annealing at different temperatures. The performances of the annealed alloys confirmed this. The $\sigma_{ts}\cdot\varepsilon_{fe}$ (ultimate tensile strength × fracture elongation) value of the cold-rolled alloy was only 23.9 GPa·%, while it was 26.6 GPa·% for the asymmetric-rolled specimen. It further increased to 27.2 GPa·% when the sample was subjected to cryorolling. This value of the alloy subjected to asymmetric cryorolling increased to 30.6 GPa·%, which was significantly higher than that for the alloy obtained by the ordinary rolling process. Furthermore, when the sample was annealed at 1073 K, the $\sigma_{ts}\cdot\varepsilon_{fe}$ value of the asymmetric-cryorolled alloy could reach up to 55.1 GPa·%. This was significantly higher than 40 GPa·% of the MEA with a three-stage heterostructure obtained from forging, conventional rolling, and annealing [59]. The result revealed that the process of asymmetric cryorolling could help improve the damage tolerance of the MEA CrCoNi.

5 Conclusions

(1) MEA CrCoNi subjected to asymmetric cryorolling showed superior mechanical properties, with an ultra-high strength of over 1.6 GPa, while maintaining a ductility of 19%.

(2) Significant heterogeneous lamellar structure was found in the alloy obtained by asymmetric cryorolling and subsequent annealing. The dislocation cell density in different lamellae was different, and there was distinct strain partitioning, forming a heterostructure material.

(3) As the annealing temperature increased, the strength of the alloy decreased, while the ductility increased significantly. When the annealing temperature was 1073 K, the asymmetric-cryorolled alloy had a high strength of nearly 1 GPa and the elongation was close to 60%.

(4) Grain distribution in alloys subjected to asymmetric cryorolling and subsequent annealing had a larger difference in grain size. The cryogenic treatment could bring more significant two-stage structural characteristics to the asymmetric-cryorolled alloys.

Acknowledgments

This work was supported by the Hunan High-Tech Industry Science and Technology Innovation Leading Plan, China (No. 2020GK2032), the Huxiang High-Level Talent Gathering Project of Hunan Province, China (No. 2018RS3015), the Innovation Driven Program of Central South University, China (No. 2019CX006), and the Research Fund of the Key Laboratory of High Performance Complex Manufacturing at Central South University, China. The authors thank Prof. Alexander P. ZHILYAEV for his deep discussion.

References

[1] MIRACLE D B, SENKOV O N. A critical review of high entropy alloys and related concepts [J]. Acta Materialia, 2017, 122: 448−511.

[2] WU Z, BEI H, PHARR G M, GEORGE E P. Temperature dependence of the mechanical properties of equiatomic solid solution alloys with face-centered cubic crystal structures [J]. Acta Materialia, 2014, 81: 428−441.

[3] GALI A, GEORGE E P. Tensile properties of high- and medium-entropy alloys [J]. Intermetallics, 2013, 39: 74−78.

[4] LAPLANCHE G, KOSTKA A, REINHART C, HUNFELD J, EGGELER G, GEORGE E P. Reasons for the superior mechanical properties of medium-entropy CrCoNi compared to high-entropy CrMnFeCoNi [J]. Acta Materialia, 2017, 128: 292−303.

[5] GLUDOVATZ B, HOHENWARTER A, THURSTON K V S, BEI Hong-bin, WU Zheng-gang, GEORGE E P, RITCHIE R O. Exceptional damage-tolerance of a medium-entropy alloy CrCoNi at cryogenic temperatures [J]. Nature Communications, 2016, 7: 10602.

[6] SATHIARAJA G D, BHATTACHARJEE P P, TSAI C W, YEH J W. Effect of heavy cryo-rolling on the evolution of microstructure and texture during annealing of equiatomic CoCrFeMnNi high entropy alloy [J]. Intermetallics, 2016, 69: 1−9.

[7] BHATTACHARJEE P P, RAY R K. Effect of processing variables on cube texture formation in powder metallurgically prepared Ni and Ni−W alloy tapes for use as substrates for coated conductor applications [J]. Materials Science and Engineering A, 2007, 459: 309−323.

[8] SUNKARI U, REDDY S R, RATHOD B D S, KUMAR S S, SAHA R, CHATTERJEE S, BHATTACHARJEE P P. Heterogeneous precipitation mediated heterogeneous nanostructure enhances strength−ductility synergy in severely cryo-rolled and annealed $CoCrFeNi_{2.1}Nb_{0.2}$ high entropy alloy [J]. Scientific Reports, 2020, 10: 1−9.

[9] REDDY S R, YOSHIDA S, BHATTACHARJEE T, SAKE N, LOZINKO A, GUO S, BHATTACHARJEE P P, TSUJI N. Nanostructuring with structural-compositional dual heterogeneities enhances strength-ductility synergy in eutectic high entropy alloy [J]. Scientific Reports, 2019, 9: 1−9.

[10] PATEL A, WANI I, REDDY S R, NARAYANASWAMY S, LOZINKO A, SAHA R, GUO S, BHATTACHARJEE P P. Strain-path controlled microstructure, texture and hardness evolution in cryo-deformed $AlCoCrFeNi_{2.1}$ eutectic high entropy alloy [J]. Intermetallics, 2018, 97: 12−21.

[11] GWALANI B, GORSSE S, CHOUDHURI D, STYLES M, ZHENG Yu-feng, MISHRA R S, BANERJEE R. Modifying transformation pathways in high entropy alloys or complex concentrated alloys via thermo-mechanical processing [J]. Acta Materialia, 2018, 153: 169−185.

[12] SHANMUGASUNDARAM T, MURTY B S, SUBRAMANYA SARMA V. Development of ultrafine grained high strength Al−Cu alloy by cryorolling [J]. Scripta Materialia, 2006, 54(12): 2013−2017.

[13] LI Chang, XIONG Han-qing, BHATTA L, WANG Lin, ZHANG Zhao-yang, WANG Hui, KONG C, YU Hai-liang. Microstructure evolution and mechanical properties of Al−3.6Cu−1Li alloy via cryorolling and aging [J]. Transactions of Nonferrous Metals Society of China, 2020, 30(11): 2904−2914.

[14] KRISHNA N N, SIVAPRASAD K, SUSILA P. Strengthening contributions in ultra-high strength cryorolled Al−4%Cu−3%TiB_2 in situ composite [J]. Transactions of Nonferrous Metals Society of China, 2014, 24(3): 641−647.

[15] ZHANG Peng-chao, SHI Jie-fu, YU Ying-shui, SUN Jun-cai, LI Ting-ju. Effect of cryorolling on microstructure and property of high strength and high conductivity Cu−0.5 wt.% Cr alloy [J]. Transactions of Nonferrous Metals Society of China, 2020, 30(9): 2472−2479.

[16] RANGARAJU N, RAGHURAM T, KRISHNA B V, RAO K P, VENUGOPAL P. Effect of cryo-rolling and annealing on microstructure and properties of commercially pure aluminium [J]. Materials Science and Engineering A, 2005, 398: 246−251.

[17] WANG Yin-ming, CHEN Ming-wei, ZHOU Feng-hua, MA

En. High tensile ductility in a nanostructured metal [J]. Nature, 2002, 419(6910): 912−915.
[18] WON J W, LEE S W, PARK S H, KANG M J, LIM K R, PARK C H, NA Y S. Ultrafine-grained CoCrFeMnNi high-entropy alloy produced by cryogenic multi-pass caliber rolling [J]. Journal of Alloys and Compounds, 2018, 742: 290−295.
[19] BHATTACHARJEE T, WANI I S, SHEIKH S, CLARK I T, OKAWA T, GUO S, BHATTACHARJEE P P, TSUJI N. Simultaneous strength−ductility enhancement of a nano-lamellar eutectic high entropy alloy by cryo-rolling and annealing [J]. Scientific Reports, 2018, 8: 3276.
[20] YU Hai-liang, LU Cheng, TIEU A K, LI Hui-jun, GODBOLE A, ZHANG Shi-hong. Special rolling techniques for improvement of mechanical properties of ultrafine-grained metal sheets: a review [J]. Advanced Engineering Materials, 2016, 18(5): 754−769.
[21] HAN Z H, LIANG S, YANG J, WEI R, ZHANG C J. A superior combination of strength-ductility in CoCrFeNiMn high-entropy alloy induced by asymmetric rolling and subsequent annealing treatment [J]. Materials Characterization, 2018, 145: 619−626.
[22] JEONG H T, KIM W J. Microstructures and mechanical properties of the non-equiatomic FeMnNiCoCr high entropy alloy processed by differential speed rolling [J]. Materials Science and Engineering A, 2018, 727: 38−42.
[23] VARVENNE C, LUQUE A, CURTIN W A. Theory of strengthening in fcc high entropy alloys [J]. Acta Materialia, 2016, 118: 164−176.
[24] OKAMOTO N L, YUGE K, TANAKA K, INUI H, GEORGE E P. Atomic displacement in the CrMnFeCoNi high-entropy alloy—A scaling factor to predict solid solution strengthening [J]. AIP Advances, 2016, 6(12): 125008.
[25] ZHAO Y L, YANG T, TONG Y, WANG J, LUAN J H, JIAO Z B, CHEN D, YANG Y, HU A, LIU C T, KAI J J. Heterogeneous precipitation behavior and stacking-fault-mediated deformation in a CoCrNi-based medium-entropy alloy [J]. Acta Materialia, 2017, 138: 72−82.
[26] SLONE C E, CHAKRABORTY S, MIAO J, GEORGE E P, MILLS M J, NIEZGODA S R. Influence of deformation induced nanoscale twinning and FCC−HCP transformation on hardening and texture development in medium-entropy CrCoNi alloy [J]. Acta Materialia, 2018, 158: 38−52.
[27] GUO Sheng, LIU C T. Phase stability in high entropy alloys: Formation of solid-solution phase or amorphous phase [J]. Progress in Natural Science: Materials International, 2011, 21(6): 433−446.
[28] FU Jian-xin, CAO Cheng-ming, TONG Wei, PENG Liang-ming. Effect of thermomechanical processing on microstructure and mechanical properties of CoCrFeNiMn high entropy alloy [J]. Transactions of Nonferrous Metals Society of China, 2018, 28(5): 931−938.
[29] ZADDACH A J, NIU C, KOCH C C, IRVING D L. Mechanical properties and stacking fault energies of NiFeCrCoMn high-entropy alloy [J]. JOM, 2013, 65(12): 1780−1789.
[30] MORAVCIK I, CIZEK J, KOVACOVA Z, NEJEZCHLEBOVA J, KITZMANTEL M, NEUBAUER E, KUBENA I, HORNIK V, DLOUHY I. Mechanical and microstructural characterization of powder metallurgy CoCrNi medium entropy alloy [J]. Materials Science Engineering A, 2017, 701: 370−380.
[31] LIANG Yao-jian, WANG Lin-jing, WEN Yu-ren, CHENG Bao-yuan, WU Qin-li, CAO Tang-qing, XIAO Qian, XUE Yun-fei, SHA Gang, WANG Yan-dong, REN Yang, LI Xiao-yan, WANG Lu, WANG Fu-chi, CAI Hong-nian. High-content ductile coherent nanoprecipitates achieve ultrastrong high-entropy alloys [J]. Nature Communications, 2018, 9(1): 4063.
[32] WANI I S, BHATTACHARJEE T, SHEIKH S, LU Y P, CHATTERJEE S, BHATTACHARJEE P P, GUO S, TSUJI N. Ultrafine-grained $AlCoCrFeNi_{2.1}$ eutectic high-entropy alloy [J]. Materials Research Letters, 2016, 4(3): 174−179.
[33] SHI Pei-jian, REN Wei-li, ZHENG Tian-xiang, REN Zhong-ming, HOU Xue-ling, PENG Jian-chao, HU Peng-fei, GAO Yan-fei, ZHONG Yun-bo, LIAW P W. Enhanced strength–ductility synergy in ultrafine-grained eutectic high-entropy alloys by inheriting microstructural lamellae [J]. Nature Communications, 2019, 10(1): 489.
[34] LAPLANCHE G, BERGLUND S, REINHART C, KOSTKA A, FOX F, GEORGE E P. Phase stability and kinetics of σ-phase precipitation in CrMnFeCoNi high-entropy alloys [J]. Acta Materialia, 2018, 161: 338−351.
[35] CAHN J W. The kinetics of grain boundary nucleated reactions [J]. Acta Metallurgica, 1956, 4: 449−459.
[36] WU Xiao-lei, YANG Mu-xin, YUAN Fu-ping, WU Gui-lin, WEI Yu-jie, HUANG Xiao-xu, ZHU Yun-tian. Heterogeneous lamella structure unites ultrafine-grain strength with coarse-grain ductility [J]. Proceedings of National Academy of Sciences of the United States of America, 2015, 112(47): 14501−14505.
[37] STEPANOV N, TIKHONOVSKY M, YURCHENKO N, ZYABKIN D, KLIMOVA M, ZHEREBTSOV S, EFIMOV A, SALISHCHEV G. Effect of cryo-deformation on structure and properties of CoCrFeNiMn high-entropy alloy [J]. Intermetallics, 2015, 59: 8−17.
[38] OKAMOTO N L, FUJIMOTO S, KAMBARA Y, KAWAMURA M, CHEN Zhenghao, MATSUNOSHITA H, TANAKA K, INUI H, GEORGE E P. Size effect, critical resolved shear stress, stacking fault energy, and solid solution strengthening in the CrMnFeCoNi high-entropy alloy [J]. Scientific Reports, 2016, 6: 35863.
[39] SATHIARAJ G D, AHMED M Z, BHATTACHARJEE P P. Microstructure and texture of heavily cold-rolled and annealed fcc equiatomic medium to high entropy alloys [J]. Journal of Alloys and Compounds, 2016, 664: 109−119.
[40] IDRISSI H, RYELANDT L, VERON M, SCHRYVERS D, JACQUES P J. Is there a relationship between the stacking fault character and the activated mode of plasticity of Fe−Mn-based austenitic steels? [J]. Scripta Materialia, 2009, 60(11): 941−944.
[41] LIU S F, WU Y, WANG H T, HE J Y, LIU J B, CHEN C X, LIU X J, WANG H, LU Z P. Stacking fault energy of face-centered-cubic high entropy alloys [J]. Intermetallics, 2018, 93: 269−273.
[42] SATHIARAJ G D, SKROTZKI W, IMMANUEL R J, PUKENAS A, SCHAARSCHUCH R, PANIGRAHI S K, CHELVANE A, KUMAR S S S. Microstructure and texture of cold rolled and recrystallized CrNoNi medium-entropy alloy [J]. Materials Science Forum. 2018, 941: 833−838.
[43] FULLMAN R L, FISHER J C. Formation of annealing twins during grain growth [J]. Journal of Applied Physics, 1951, 22(11): 1350−1355.
[44] OTTO F, HANOLD N L, GEORGE E P. Microstructural evolution after thermomechanical processing in an equiatomic, single-phase CoCrFeMnNi high-entropy alloy with special focus on twin boundaries [J]. Intermetallics, 2014, 54: 39−48.

[45] BHATTACHARJEE P P, SINHA S K, UPADHYAYA A. Effect of sintering temperature on grain boundary character distribution in pure nickel [J]. Scripta Materialia, 2007, 56: 13−16.
[46] WU S W, WANG G, YI J, JIA Y D, HUSSAIN I, ZHAI Q J, LIAW P K. Strong grain-size effect on deformation twinning of an $Al_{0.1}$CoCrFeNi high-entropy alloy [J]. Materials Research Letters, 2017, 5(4): 276−283.
[47] MEYERS M A, MISHRA A, BENSON D J. Mechanical properties of nanocrystalline materials [J]. Progress Materials Science, 2006, 51(4): 427−556.
[48] ZENG Zhi, LI Xiao-yan, XU Dong-shemg, LU Lei, GAO Hua-jian, ZHU Ting. Gradient plasticity in gradient nano-grained metals [J]. Extreme Mechanics Letters, 2016, 8: 213−219.
[49] WU Xiao-lei, ZHU Yun-tian. Heterogeneous materials: A new class of materials with unprecedented mechanical properties [J]. Materials Research Letters, 2017, 5(8): 527−532.
[50] ASHBY M F. The deformation of plastically non-homogeneous materials [J]. Philosophical Magazine, 1970, 21(170): 399−424.
[51] FU Zhi-qiang, MACDONALD B E, LI Zhi-ming, JIANG Zhen-fei, CHEN Wei-ping, ZHOU Yi-zhang, LAVERNIA E J. Engineering heterostructured grains to enhance strength in a single-phase high-entropy alloy with maintained ductility [J]. Materials Research Letters, 2018, 6(11): 634−640.
[52] CHEN G, QIAO J W, JIAO Z M, ZHAO D, ZHANG T W, MA S G, WANG Z H. Strength-ductility synergy of $Al_{0.1}$CoCrFeNi high-entropy alloys with gradient hierarchical structures [J]. Scripta Materialia, 2019, 167: 95−100.
[53] SLONE C E, MIAO J, GEORGE E P, MILLS M J. Achieving ultra-high strength and ductility in equiatomic CrCoNi with partially recrystallized microstructures [J]. Acta Materialia, 2019, 165: 496−507.
[54] YOSHIDA S, BHATTACHARJEE T, BAI Yu, TSUJI N. Friction stress and Hall−Petch relationship in CoCrNi equi-atomic medium entropy alloy processed by severe plastic deformation and subsequent annealing [J]. Scripta Materialia, 2017, 134: 33−36.
[55] XIA Wei-jun, CHEN Zhen-hua, CHEN Ding, ZHU Su-qing. Microstructure and mechanical properties of AZ31 magnesium alloy sheets produced by differential speed rolling [J]. Journal of Materials Processing Technology, 2009, 209(1): 26−31.
[56] MA R, WANG L, WANG Y N, ZHOU D Z. Microstructure and mechanical properties of the AZ31 magnesium alloy sheets processed by asymmetric reduction rolling [J]. Materials Science and Engineering A, 2015, 638: 190−196.
[57] SARMA V S, WANG J, JIAN W W, KAUFFMANN A, CONRAD H, FREUDENBERGER J, ZHU Y T. Role of stacking fault energy in strengthening due to cryo-deformation of FCC metals [J]. Materials Science and Engineering A, 2010, 527: 7624−7630.
[58] YU Hai-liang, YAN Ming, LI Jin-tao, GODBOLE A, LU Cheng, TIEU K, LI Hui-jun, KONG C. Mechanical properties and microstructure of a Ti−6Al−4V alloy subjected to cold rolling, asymmetric rolling and asymmetric cryorolling [J]. Materials Science and Engineering A, 2018, 710: 10−16.
[59] YANG Mu-xin, YAN Ding-shun, YUAN Fu-ping, JIANG Ping, MA Evan, WU Xiao-lei. Dynamically reinforced heterogeneous grain structure prolongs ductility in a medium-entropy alloy with gigapascal yield strength [J]. Proceedings of the National Academy of Sciences of the United States of America, 2018, 115(28): 7224−7229.

深冷异步轧制制备高力学性能 CrCoNi 中熵合金

吴雨泽[1,2,3]，张朝阳[1,2,3]，刘 娟[1,2,3]，Charlie KONG[4]，
Yu WANG[4]，Puneet TANDON[5]，Alexander PESIN[6]，喻海良[1,2,3]

1. 中南大学 高性能复杂制造国家重点实验室，长沙 410083；
2. 中南大学 机电工程学院，长沙 410083；3. 中南大学 轻合金研究院，长沙 410083；
4. Mark Wainwright Analytical Centre, University of New South Wales, Sydney, NSW 2052, Australia;
5. PDPM Indian Institute of Information Technology, Design and Manufacturing, Jabalpur 482005, India;
6. Laboratory of Mechanics of Gradient Nanomaterials,
Nosov Magnitogorsk State Technical University, Magnitogorsk 455000, Russia

摘 要：为了获得具有更好强塑性平衡的 CrCoNi 中熵合金，采用冷轧、异步轧制、深冷轧制和深冷异步轧制 4 种工艺对中熵合金 CrCoNi 进行加工，并对合金进行不同温度的退火处理。研究结果表明：深冷异步轧制的合金获得超过 1.6 GPa 的高强度，当经过 1073 K 的退火处理后，在具有接近 60%的伸长率的同时，仍然保留接近 1 GPa 的强度。采用深冷异步轧制和退火后，得到较室温异步轧制更为明显的异质特征，这使材料具有更高的强度与更好的塑性。

关键词：中熵合金；异质结构；退火；力学性能；深冷异步轧制

(Edited by Bing YANG)